

A Continuous Pump-Probe Experiment to Observe Rydberg Wave Packet Dynamics

K. L. Romans,¹ K. Foster,¹ S. Majumdar,¹ B. P. Acharya,¹ O. Russ,¹ A. H. N. C. De Silva,¹ and D. Fischer¹

¹*Physics Department and LAMOR, Missouri University of Science & Technology, Rolla, MO 65409, USA*

(Dated: February 11, 2025)

Rydberg atoms remain in the limelight due to their applications in quantum optics and information technologies. In this work, the dynamics of Rydberg atoms stored in a momentum spectrometer by an all-optical trap is studied by ionizing them in the field of a continuous wave optical dipole trap. While the addition of the optical dipole trap allows to further cool the atoms, it comes at the expense of the time of flight information which is required to retrieve photoelectron momentum distributions. Here, we report on a method that extends the standard COLTRIMS (cold target recoil ion momentum spectroscopy) technique, including continuous wave lasers in pump-probe schemes, by utilizing coincidence measurements. In particular, the photoionization of atomic ${}^6\text{Li}$ initially in a spin-polarized $2^2P_{3/2}$ state is explored. Multi-photon excitation from a tunable-mode femtosecond pulse is exploited to produce Rydberg atoms, which can then be ionized by the dipole field. The resulting ionization rate becomes explicitly time-dependent, and analyzing its structure unlocks the real-time atomic dynamics on nanosecond time scales.

Time-resolved laser spectroscopy, along with high-resolution momentum imaging, provides detailed insights into the dynamics of atomic or molecular systems. Femtosecond pump-probe schemes were pioneered by A. Zewail [1] and they evolved into the gold standard for time-resolved spectroscopy. They were extensively used to study nuclear dynamics in molecular reactions on a femtosecond timescale (e.g. [2]). Shorter time scales became accessible with the availability of attosecond laser pulses created by high-harmonic generation [3–5] using streaking [6, 7], pump-probe [8–10], or the interferometric RABBITT [7, 11–13] techniques. Nowadays, there is a wealth of time-resolved methods exploiting different types of light sources ranging from accelerator-sized free-electron lasers, to compact tabletop laser devices employing advanced pulse shaping techniques, and spanning time-scales from the attosecond to the picosecond time regime.

In this letter, we extend the toolbox for time-resolved photoelectron spectroscopy by introducing a technique that is particularly simple and suited to studying slow nanosecond dynamics. In contrast to conventional pump-probe schemes, where the time information is obtained by scanning the delay between two pulses, we use a femtosecond pulse pump and a weak continuous wave (cw) probe; the latter can photoionize the excited atomic system at any time after the former. A cold target recoil ion momentum spectrometer (COLTRIMS) [14–17] is employed to detect photoelectrons and recoiling target ions in coincidence. In conventional COLTRIMS, the time information of the target ionization is required to calculate the fragments' momentum vectors. Although the atoms' time of ionization is not directly measurable within the continuous wave, we can recover this information by exploiting the fact that the total momentum of all the target fragments is zero after photoionization (neglecting the very small photon momentum). This approach does not only retain the photoelectron energy and angular dis-

tributions, but it also provides additional information on the time evolution of the wave packet that is formed by the pump pulse. This method allows measurements of the electron's motion as it occurs in energetically narrow wave packets, e.g., in Rydberg atoms; such systems are important in the development and study of coherent control schemes in ultra-cold atomic samples (e.g., [18, 19]).

For this experiment, we measure the time evolution of magnetic Rydberg wave packets in a weak external field. Atomic ${}^6\text{Li}$ gas is suspended in the laser light of a near-resonant all-optical trap (AOT) [20]. The AOT's configuration optically pumps the system, resulting in a population of about 25% in the excited $2^2P_{3/2}(F = 5/2)$ hyperfine state. Upwards of 93% of these excited atoms populate a single angular magnetic sublevel, $m_\ell = -1$, with respect to the quantization axis given by the spectrometer's magnetic field and corresponding z -axis.

To populate the Rydberg states, a femtosecond light source was used, similar to that described in [21, 22], which is a commercially available optical parametric chirped-pulse amplifier (OPCPA). At its heart is a Ti:Sa oscillator which provides a broadband seed-signal for two noncollinear optical parametric amplifier (NOPA) stages. For this study, the light source was tuned to emit pulses with a central wavelength, pulse width, and repetition rate of 735 ± 10 nm, 50 fs, and 200 kHz, respectively. Unlike previous experiments (e.g. [23, 24]), the intensity of this source was kept below the threshold of direct few-photon ionization with a peak intensity of up to 10^{11} W/cm². This beam is intersected with the AOT at an angle of 12.5° with respect to the z -axis. Finally, an optical dipole trap (ODT) is generated using an industrial grade ytterbium-doped fiber laser, which outputs a infrared continuous wave at 1070 ± 5 . This beam's polarization and propagation directions lie in the xy -plane, and it reaches the reaction volume with an intensity of about 10^7 W/cm².

Standard reaction microscopes (ReMi) rely crucially

on the timing information provided by a pulsed source. Each recoil-ion's and electron's time of flight $T_{r/e}$ is measured with respect to the clock set by it. Presently, the ionization is triggered by photoabsorption in a continuous field causing the time information to become lost, as atoms can be ionized at any time between pulses. To overcome this hurdle, we take advantage of aspects of the photoionization process, atomic target, and spectrometer geometry. The fragments are measured in coincidence (e.g. [15]), which restricts their time of flight difference $\Delta T (\equiv T_r - T_e)$ to a measurable, few nanosecond wide distribution. Given the low temperature of the atom cloud and the negligible momentum of the ionizing photon, we can set the total momentum of each ion-electron pair to zero [25].

In detail, the charged fragments are drawn in opposite directions towards the particle detectors in the spectrometer by homogeneous electric and magnetic fields, arranged along the longitudinal z -axis. Thereby, the particles (charge q) undergo a cyclotron motion in the magnetic field B_z due to the Lorentz force, i.e., the x and y positions of particles with the initial momentum components p_x and p_y , after a time-of-flight T are [17],

$$x = \frac{1}{qB_z} [\sin(\omega_c T) p_x + (1 - \cos(\omega_c T)) p_y], \quad (1)$$

$$y = \frac{1}{qB_z} [(\cos(\omega_c T) + 1) p_x + \sin(\omega_c T) p_y]. \quad (2)$$

The key to the present time derivation method is that the fragments' motion in the spectrometer's electromagnetic field is highly asymmetric due to the recoil-ion being considerably more massive than its photoelectron. While their momenta are equal in magnitude, the recoil-ions' kinetic energies are more than 5 orders of magnitude smaller than that of their electrons. It is interesting to note, that the time of flight distributions of electrons and ions (which are not directly measured in our experiment) have about the same width (around one hundred nanoseconds), while their absolute travel time can differ by more than a factor of hundred. Due to the recoil-ions' large inertia, their cyclotron frequency $\omega_c (\equiv qB_z/m)$ is so small that the rotational phase $\omega_c T$, from the above equations, varies less than 1% of 2π ; the ions' phase distribution can thus be approximated by a constant.

The much lighter electrons, in contrast, undergo several full cyclotron revolutions before hitting the detector, and the final rotational phases $\omega_c T$ depend strongly on the electrons' initial momenta. In essence, the electrons' rotational phase and, therefore, their time of flight is encoded in the relative positions of recoil ions and electrons on their respective detectors. If the phase variation does not exceed 2π , then the electrons' travel time can be unambiguously recovered and the three-dimensional electron momentum vectors derived.

Details on this method can be found in [22, 26], where an excellent correspondence between directly measured

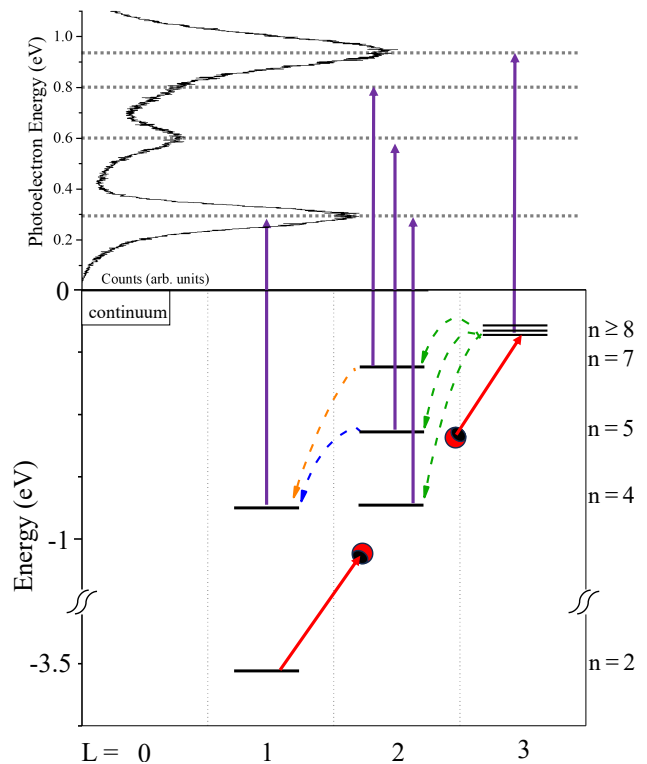


FIG. 1. Recovered photoelectron energy spectrum (top) and associated dipole-allowed energy diagram (bottom). Femtosecond and ODT photons are shown with red and purple solid arrows respectively, while the dominant spontaneous decay channels are dashed.

and derived times of flight was observed. Once recovered, this time can be used in to calculate the resultant energy and momentum distributions (see tops of Fig. 1 and Fig. 3, respectively). During an experimental run, the atoms are excited by absorption of two circularly polarized fs-photons into a maximally aligned f -state wavepacket involving Rydberg states with $n \geq 8$. The excited wavepacket is then allowed to decay spontaneously back towards the ground state. During this decay, the ODT is continuously ionizing the atoms with a single photon. Energy conservation can then be used to associate peaks in the photoelectron energy distribution to internal bound states (Fig. 1, bottom).

With the time of ionization, a whole domain of time-dependent phenomena can be investigated. An example is the slow μs population dynamics driven by spontaneous decay cascades. By focusing on the set of dominant spontaneous decay channels it becomes straightforward to extract the explicit inter-state population dynamics in an effective real-time scheme [26].

The nanosecond accuracy also allows for the exploration of faster atomic dynamics (~ 1 ns), which can be seen in Fig. 2. Here, the ionization rate is plotted as a function of photoelectron energy and the derived time of ionization. The ionization rate features a periodic time

dependence throughout the whole energy range. Two dominant streaks appear, which can be associated with the $n = 4$ states on the left and the Rydberg superposition on the right. Comparing with Fig. 1, the 5D and 7D states can be seen at around 0.6 and 0.8 eV, respectively; the remaining weaker lines come from the copious intermediate states in the cascade and are not shown along with the dominant decay channels.

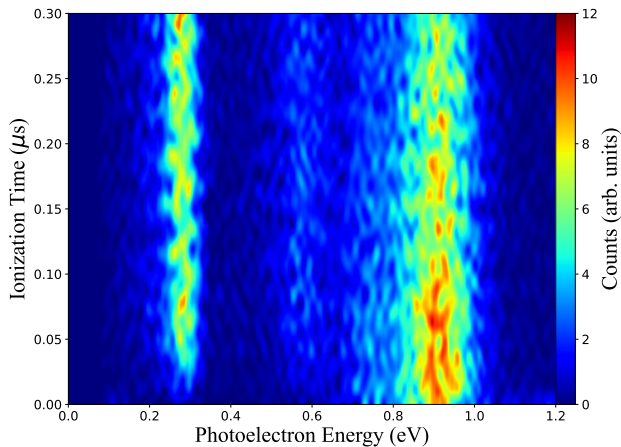


FIG. 2. Derived time of ionization vs. photoelectron energy with the z -axis corresponding to ionization rate. Note how a periodic time dependence permeates all energies.

This experimental data can be explained with the simple model shown in Fig. 3. The atoms are exposed to the homogeneous magnetic spectrometer field oriented along the z -axis. The circularly polarized femtosecond laser beam is guided through the chamber in the yz -plane exciting the atoms to a Rydberg wavepacket. This momentarily maintains the alignment of the atoms' mean magnetic moment $\langle \vec{\mu} \rangle$ along the photons' propagation direction. Since this moment has a component perpendicular to the magnetic field the system will undergo Larmor precession in the xy -plane. Meanwhile, the atoms have sufficient energy to absorb a single infrared photon from the ODT field and be ionized. The infrared photon propagates along the y -axis, with its linear polarization along the x , shown in purple. The probability of ionizing the atom depends on the relative orientation of this photon's polarization and the projected atomic moment. Given the geometry in the projection plane, two maxima and two minima are expected per cycle, corresponding to those times when the mean magnetic moment is aligned or perpendicular to the polarization axis, respectively.

Formally, the excited wavepacket begins in aligned f -states, i.e. $|m_\ell| = 3$. The alignment is tilted by 12.5° with respect to the z -axis, i.e., the state can be expressed as a superposition of the $|m_z| \leq 3$ magnetic sublevels, as shown in Fig. 3. This excited state can be given as the

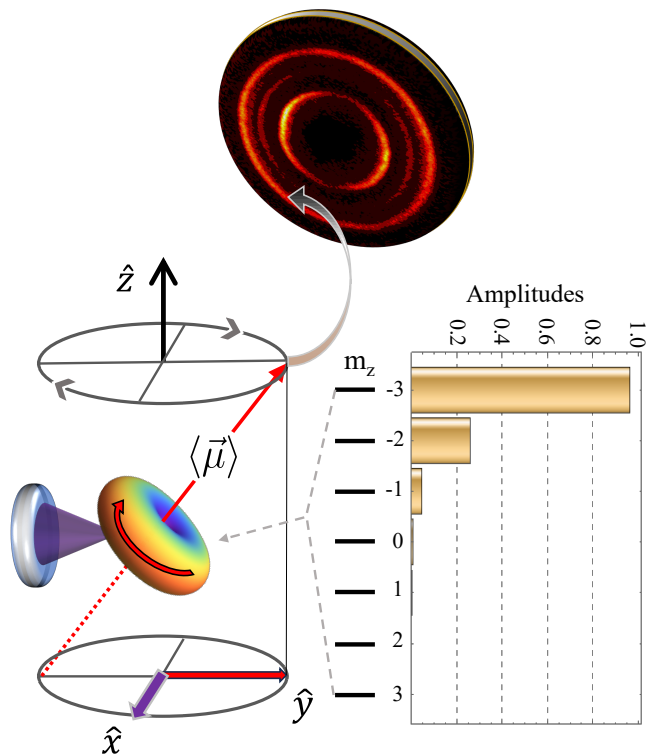


FIG. 3. Semi-classical rotating magnetic moment with exaggerated tilt angle (left), initial quantum magnetic sublevel distribution (right), and the recovered photoelectron transverse momentum distribution (top). Note how the momentum ring radii correspond to the major peaks in the energy spectrum of Fig. 1.

following sum,

$$|\psi_{\text{ex.}}(t)\rangle = \sum_{n \geq 8}^{n_{\text{max}}} \sum_{m_z = -3}^3 c_{m_z}^{(n)} \exp(-i\Omega_{m_z}^{(n)} t) |n, 3, m_z\rangle, \quad (3)$$

where the $c_{m_z}^{(n)}$ and $\Omega_{m_z}^{(n)}$ are the expansion amplitudes and eigenenergy angular frequencies, respectively, while the $|n, 3, m_z\rangle$ are the bound lithium f -orbitals.

The ionization rate from this state into a final continuum state $|\psi_{\varepsilon, \ell_f}\rangle$ can be calculated using the equation of [27],

$$R_{\text{ex.}}(t) \propto |\langle \psi_{\varepsilon, \ell_f} | D_\lambda | \psi_{\text{ex.}}(t) \rangle|^2, \quad (4)$$

where $D_\lambda (\equiv \boldsymbol{\epsilon} \cdot \mathbf{r})$ is the electric dipole operator, and (ε, ℓ_f) is the final state energy and angular momentum. When Eqs. (3) and (4) are combined, and the matrix element is integrated over the solid angle of the ejected photoelectron, the dominant time-dependent term becomes,

$$R_{\text{ex.}}(t) \propto 1 - A \cos(2 \cdot (\Omega_{-3} - \Omega_{-1}) t) + \dots, \quad (5)$$

with A being a relative amplitude. In other words, the energy difference between the $m_z = -3$ and -1 magnetic

sublevels drive the time variation of the ionization rate, with the next leading term, which depends on $m_z = -2$ and 0, being two orders of magnitude smaller. Since the states in the superposition have nearly identical eigenenergies, i.e. $\Omega_{m_z}^{(n)} \approx \Omega_{m_z}^{(n')}$, they will oscillate in phase for a few microseconds.

In order to use this model and test its accuracy, the shifts of the energy state frequencies $\Omega_{m_z}^{(n)}$ must be calculated for different magnetic sublevels. Naively, one would expect that the m_z -dependence of these shifts arises only due to the Zeeman shift, which is $m_z \cdot \omega_L$ in terms of the Larmor frequency $\omega_L (\propto B_z)$. As it turns out, this naive assumption produces a calculated frequency two times too small, as compared to data fits.

However, besides coupling the atoms to the continuum via ionization, the ODT field can also couple lower-lying bound states via the Autler-Townes effect [28]. These energy shifts can be approximated as a sum over two-state terms, $\Delta E_{AT}^{(n)} \approx \sum_{n'} \Delta E_{n,n'}$, for each of the dipole-allowed transitions between the $n'D$ -states and nF -Rydberg levels. In the large detuning limit this coupling is given as [29, 30],

$$\Delta E_{n,n'} = -\frac{I_0}{2\epsilon_0 \hbar c} \frac{|\langle \psi_{nF} | D_\lambda | \psi_{n'D} \rangle|^2}{\delta_{n,n'}}, \quad (6)$$

where $\delta_{n,n'}$ is detuning of the laser frequency with respect to the atomic transition, and I_0 is the ODT's intensity. Including the Zeeman and Autler-Townes effects in the calculated energy shifts leads to the predicted frequency picking up the missing factor of two and more closely mirroring the fits. The results of the calculation can be seen in Fig. 4, where a thin energy slice, corresponding to photoelectron energies of the Rydberg state, was explored. Assuming a single $8F$ Rydberg state, the model captures the oscillation frequency of ≈ 27 MHz. The overall intensity drops over time due to spontaneous decay.

With the success of this simple model, it begs the question as to the source of the periodicity in the remaining energy levels. While the Rydberg states are excited coherently by the femtosecond laser, the lower-lying levels are populated predominately by incoherent spontaneous decay. Such a process should quickly destroy the phase information contained in the Rydberg superposition as it gets dispersed amongst the cascade. Despite this, the $n = 4$ states near the 0.3 eV peak retain a strong periodicity and seem to hold coherence throughout the experimental run.

This is explained based on relative timescales. The excited Rydberg states are comparably long-lived, and their ionization rate in the ODT field is comparably small (~ 0.5 MHz); their time dependence is an expression of the states' evolution. The $n = 5, 7$ states have rates roughly 10-fold higher, while the $n = 4$ states are 10-fold higher still. This leads to the middle states having a time

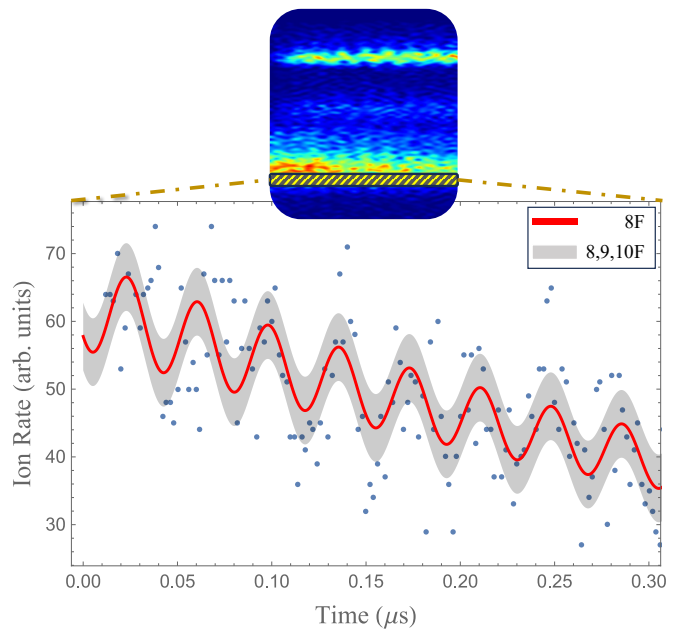


FIG. 4. Data and model curves for associated excited Rydberg states. The simplified single-state model is shown in red, while possible three-state superpositions are represented by the gray area.

dependence that is a mix of the decay channels and the driving ODT field, while the short-lived states are ionized almost as soon as they are populated. Consequently, any time-dependence seen in the $n = 4$ ionization data must be a delayed, but direct, projection of that seen in the Rydberg levels. The phase shift seen on the left and right sides of the $n = 4$ data can also be explained by the $4P$ and $4D$ channels seen in Fig. 1; the former goes through a delayed path with the 5 and 7D states, while the latter has a direct dipole-allowed path to the excited Rydberg states.

Initially intuitively pleasing, the current model is not without shortcomings. First, the spectrometer's resolution limits which states can be distinguished. The closely spaced Rydberg states are difficult to disentangle and lead to challenges when developing the analytic model. Second, only those states in the dominant decay channels (see Fig. 1) are considered for the Autler-Townes shift. Bound state spontaneous decay constants were calculated using the Alkali Rydberg Calculator (ARC) [31] at each step of the cascade, and weak couplings were neglected. Finally, although the coupling to the lower-lying bound states was included for the Autler-Townes effect, the continuum coupling was not. Sometimes referred to as the electron's ponderomotive, or quiver, energy, this effect further shifts the energy levels due to an intense laser field. Presently, the low intensity of the ODT field allows for this shift to be safely ignored, but it may need more careful consideration in future studies.

In conclusion, we have demonstrated a method of

derived time that allows for the investigation of time-dependent atomic processes in real time. Born out of necessity, this technique utilizes the continuous field of an infrared ODT laser, in conjunction with a pulsed femtosecond pump, to constantly probe the energy states of the atoms. Lithium-6 atoms initially in a spin-polarized $2^2P_{3/2}$ state are excited by the fs-pump into similarly aligned f -states. This excitation forms a coherent superposition of Rydberg states, which then couples to the ODT's and spectrometer's fields. This results in shifts in the atomic energy levels via the Zeeman and Autler-Townes effects. Furthermore, the axis of alignment is slightly tilted with respect to the spectrometer's z -axis. This adds to the mix a superposition of magnetic sub-levels or a magnetic wave packet. Each wave packet, and its associated mean magnetic moment, is dressed by the ODT's field and undergoes an enhanced Larmor precession. In this way, the ionization rate becomes explicitly time-dependent, and through its analysis, both the relatively slow population and faster wave packet dynamics become unlocked.

The ionization scheme presented here is suited to study the dynamics of many atomic Alkali systems. Particular interest has been placed on Rydberg atoms given their recent return into the proverbial limelight as vehicles for information technology. Along the way, great effort has been taken to focus on dipole-allowed configurations, due to the ease of the framework, but a tremendous amount of physics lies just beyond the forbidden. Recent work into orbital angular momentum (OAM) light beams (e.g. [32]) have demonstrated a convenient source of photons with angular quantum number $\ell \geq 2$. When used with atomic targets, one must take great pains to keep the atoms on the OAM beam's axis of symmetry, such that the angular momentum transfer remains well-defined; atoms have such a small spatial extent, relative to the OAM beam, that they experience an effective plane wave otherwise. In contrast, Rydberg atoms can easily have wave functions that extend out to a few hundred atomic units. This leaves Rydberg atoms as prime targets to couple to OAM fields for dipole-forbidden investigations. This work, in conjunction with [22, 26], not only demonstrates an accessible source of Alkali Rydberg atoms for many ongoing COLTRIMS experiments but also a way in which to probe their dynamics continuously.

The experimental material presented here is based on work supported by the National Science Foundation under Grants No. PHY-2207854 and No. PHY-1554776.

[1] A. H. Zewail, *The Journal of Physical Chemistry A* **104**, 5660 (2000).
 [2] A. Stolow, A. E. Bragg, and D. M. Neumark, *Chemical Reviews* **104**, 1719 (2004).
 [3] P. B. Corkum and F. Krausz, *Nature Physics* **3**, 381

(2007).
 [4] M. F. Kling and M. J. Vrakking, *Annual Review of Physical Chemistry* **59**, 463 (2008).
 [5] F. Krausz and M. Ivanov, *Reviews of Modern Physics* **81**, 163 (2009).
 [6] J. Itatani, F. Quéré, G. L. Yudin, M. Y. Ivanov, F. Krausz, and P. B. Corkum, *Physical Review Letters* **88**, 173903 (2002).
 [7] L. Cattaneo, J. Vos, M. Lucchini, L. Gallmann, C. Cirelli, and U. Keller, *Optics Express* **24**, 29060 (2016).
 [8] P. Tzallas, E. Skantzakis, L. A. A. Nikolopoulos, G. D. Tsakiris, and D. Charalambidis, *Nature Physics* **7**, 781 (2011).
 [9] R. Geneaux, H. J. B. Marroux, A. Guggenmos, D. M. Neumark, and S. R. Leone, *Philosophical Transactions of the Royal Society A: Mathematical, Physical and Engineering Sciences* **377**, 20170463 (2019).
 [10] J. Duris, S. Li, T. Driver, E. G. Champenois, J. P. MacArthur, A. A. Lutman, Z. Zhang, P. Rosenberger, J. W. Aldrich, R. Coffee, G. Coslovich, F.-J. Decker, J. M. Glowina, G. Hartmann, W. Helml, A. Kamalov, J. Knurr, J. Krzywinski, M.-F. Lin, J. P. Marangos, M. Nantel, A. Natan, J. T. O'Connell, N. Shivaram, P. Walter, A. L. Wang, J. J. Welch, T. J. A. Wolf, J. Z. Xu, M. F. Kling, P. H. Bucksbaum, A. Zholents, Z. Huang, J. P. Cryan, and A. Marinelli, *Nature Photonics* **14**, 30 (2019).
 [11] P. M. Paul, E. S. Toma, P. Breger, G. Mullot, F. Auge-ü, P. Balcou, H. G. Muller, and P. Agostini, *Science* **292**, 1689 (2001).
 [12] H. Muller, *Applied Physics B* **74**, s17 (2002).
 [13] L. Cattaneo, L. Pedrelli, R. Y. Bello, A. Palacios, P. D. Keathley, F. Martín, and U. Keller, *Physical Review Letters* **128**, 063001 (2022).
 [14] J. Ullrich, R. Moshhammer, A. Dorn, R. Dörner, L. P. H. Schmidt, and H. Schmidt-Böcking, *Reports on Progress in Physics* **66**, 1463 (2003).
 [15] R. Moshhammer, D. Fischer, and H. Kollmus, in *Many-Particle Quantum Dynamics in Atomic and Molecular Fragmentation* (Springer Berlin Heidelberg, 2003) pp. 33–58.
 [16] D. Fischer, D. Globig, J. Gouillon, M. Grieser, R. Hubele, V. L. B. de Jesus, A. Kelkar, A. LaForge, H. Lindenthal, D. Misra, B. Najjari, K. Schneider, M. Schulz, M. Sell, and X. Wang, *Physical Review Letters* **109**, 113202 (2012).
 [17] D. Fischer, in *Ion-Atom Collisions*, edited by M. Schulz (De Gruyter, 2019) pp. 103–156.
 [18] N. Takei, C. Sommer, C. Genes, G. Pupillo, H. Goto, K. Koyasu, H. Chiba, M. Weidemüller, and K. Ohmori, *Nature Communications* **7**, 10.1038/ncomms13449 (2016).
 [19] A. Devolder, P. Brumer, and T. V. Tscherbul, *Physical Review Letters* **126**, 153403 (2021).
 [20] S. Sharma, B. P. Acharya, A. H. N. C. De Silva, N. W. Parris, B. J. Ramsey, K. L. Romans, A. Dorn, V. L. B. de Jesus, and D. Fischer, *Physical Review A* **97**, 043427 (2018).
 [21] A. Harth, C. Guo, Y.-C. Cheng, A. Losquin, M. Miranda, S. Mikaelsson, C. M. Heyl, O. Prochnow, J. Ahrens, U. Morgner, A. L'Huillier, and C. L. Arnold, *J. Opt.* **20**, 014007 (2017).
 [22] K. L. Romans, *Photoionization of spin-polarized Rydberg atoms out of a continuous wave optical dipole trap*,

- phdthesis, Missouri S&T (2023).
- [23] A. H. N. C. De Silva, D. Atri-Schuller, S. Dubey, B. P. Acharya, K. L. Romans, K. Foster, O. Russ, K. Compton, C. Rischbieter, N. Douguet, K. Bartschat, and D. Fischer, *Physical Review Letters* **126**, 023201 (2021).
- [24] B. P. Acharya, M. Dobson, S. Dubey, K. L. Romans, A. H. N. C. De Silva, K. Foster, O. Russ, K. Bartschat, N. Douguet, and D. Fischer, *Phys. Rev. A* **104**, 053103 (2021).
- [25] R. Hubele, M. Schuricke, J. Goullon, H. Lindenblatt, N. Ferreira, A. Laforge, E. Brühl, V. L. B. de Jesus, D. Globig, A. Kelkar, D. Misra, K. Schneider, M. Schulz, M. Sell, Z. Song, X. Wang, S. Zhang, and D. Fischer, *Review of Scientific Instruments* **86**, 033105 (2015).
- [26] K. L. Romans, A. H. N. C. De Silva, B. P. Acharya, K. Foster, O. Russ, and D. Fischer, *A pump-probe experiment in cw-mode on ionization of rydberg atoms* (2023).
- [27] A. F. Starace, Springer handbook of atomic, molecular, and optical physics (Springer New York, 2006) Chap. 24, pp. 379–382.
- [28] S. H. Autler and C. H. Townes, *Physical Review* **100**, 703 (1955).
- [29] M. Haas, U. D. Jentschura, and C. H. Keitel, *American Journal of Physics* **74**, 77 (2006).
- [30] I. V. Hertel and C.-P. Schulz, *Atoms, Molecules and Optical Physics I: Atoms and Spectroscopy* (Springer Berlin Heidelberg, 2015).
- [31] N. Šibalić, J. Pritchard, C. Adams, and K. Weatherill, *Computer Physics Communications* **220**, 319 (2017).
- [32] Y. Fang, Z. Guo, P. Ge, Y. Dou, Y. Deng, Q. Gong, and Y. Liu, *Light: Science and Applications* **11**, 10.1038/s41377-022-00726-7 (2022).